Downscaling MODIS Land Surface Temperature Product Using an Adaptive Random Forest Regression Method and Google Earth Engine for a 19-Years Spatiotemporal Trend Analysis Over Iran

Hamid Ebrahimy, Hossein Aghighi, Mohsen Azadbakht, Meisam Amani, *Senior Member, IEEE*, Sahel Mahdavi, and Ali Akbar Matkan

***Abstract*—MODIS land surface temperature (LST) product (MOD11A1) has been widely used in analysing spatiotemporal trends of LST. However, its applicability is limited, partially due to its coarse spatial resolution (i.e., 1 km). In this study, an Adaptive random forest regression (ARFR) method was developed for LST downscaling at national scale. This study also provided a framework to shift from downscaling single-time image sets to extensive time-series of MOD11A1 LST images in an operational approach (i.e., a 19-years spatiotemporal LST trend analysis over Iran) using the Google Earth Engine (GEE) cloud computing platform. The performance of ARFR was assessed by comparing the results of the downscaled LSTs with the Landsat-8 LST data on different dates of six consecutive years (2014–2019) over ten different sub-areas in Iran. The results demonstrated the effectiveness of the proposed method with an average root mean square error and mean absolute error of 2.22 °C and 1.59 °C, respectively. The results of spatiotemporal LST trend analysis showed that 25.08%, 10.05%, 56.68%, 1.04%, and 32.84% of Iran experienced significant positive trends during a full year, spring, summer, fall, and winter, respectively. Significant negative trends were also observed over the 3.09%, 23.84%, 7.54%, 17.38%, and 18.77% of Iran during a full year, spring, summer, fall, and winter, respectively. In summary, the outcomes of this study not only exhibit the spatiotemporal trends of LST across Iran, but also reveal the substantial benefits of the ARFR method in downscaling LST using GEE.**

***Index Terms*—Adaptive random forest, downscaling, Google Earth Engine (GEE), land surface temperature (LST), MODIS, trend analysis.**

I. Introduction

REMOTELY sensed land surface temperature (LST) data is a unique source of information in climate change studies. Climate change has significant impacts on environmental conditions and human activities around the globe [1]. One of the fundamental issues related to the climate change is severe changes in LST of the earth's surface [2], [3]. This issue has negatively affected several regions of the world, especially dry countries, such as Iran [4]–[6]. Thus, it is required to investigate the spatiotemporal trend of LST changes over a long period of time to obtain a better understanding of LST evolution in the earth's surface [7], [8].

The spatiotemporal variations of LST significantly depend on the geographic location, topographic characteristics, soil moisture, solar geometry, atmospheric conditions, and land cover type [9]–[11]. Therefore, the spatiotemporal dynamics of LST has been considered a key variable for modeling and understanding the exchange of energy and water between the earth's surface and atmosphere from local to global scales [12], [13]. It has also been successfully utilized for investigating different earth surface processes, such as land cover changes [14], [15], urban climate analysis [16], [17], and drought severity assessment [18]. Thus, due to spatiotemporal variations of LST, the investigation should be conducted in both spatial and temporal contexts.

Remotely sensed thermal images, with frequent revisits and global coverage at various spatial resolutions, are known as the key sources of information for spatiotemporal LST analysis [2], [3], [19]–[21]. The frequent satellite observations facilitate trend analysis and provide more consistent results in the spatiotemporal LST analysis. However, the tradeoff between spatial and temporal resolutions of thermal satellite images brings a challenge to explore the LST variations either at high spatial or at high temporal resolutions. To overcome this limitation, downscaling coarse-resolution LST data has become a common solution in recent years [22]–[24].

Downscaling methods are often used to improve the spatial resolution of LST products through utilizing ancillary variables that can be acquired at finer spatial resolutions. A variety of approaches have been adopted for LST downscaling, ranging from statistical and machine learning (ML) techniques [25]–[29] to physical methods [30] and spatiotemporal approaches [31], [32]. In recent years, statistical and ML methods have received huge attention in LST downscaling studies [24], [27]. In this regard, random forest regression (RFR) has demonstrated a high potential for LST downscaling because of its good adaptability

Manuscript received August 23, 2020; revised November 28, 2020; accepted January 7, 2021. Date of publication January 13, 2021; date of current version February 3, 2021. *(Corresponding author: Meisam Amani.)*

Hamid Ebrahimy, Hossein Aghighi, Mohsen Azadbakht, and Ali Akbar Matkan are with the Center for Remote Sensing and GIS Research, Faculty of Earth Sciences, Shahid Beheshti University, Tehran 1983969411, Iran (e-mail: h_ebrahimy@sbu.ac.ir; h_aghighi@sbu.ac.ir; m_azadbakht@sbu.ac.ir; a-matkan@sbu.ac.ir).

Meisam Amani and Sahel Mahdavi are with the Wood Environment and Infrastructure Solutions, Ottawa, ON K2E7L5, Canada (e-mail: meisam.amani@woodplc.com; sahel.mahdavi@woodplc.com).

Digital Object Identifier 10.1109/JSTARS.2021.3051422

and high accuracy [33]–[35]. For example, Hutengs and Vohland [34] successfully adopted RFR to downscale MODIS LST product at regional scales. According to the authors, the RFR method provided superior performance in comparison with the benchmark methods. Following that research, Yang *et al*. [35] used RFR regression based on the spectral indices to downscale MODIS LST product over arid regions in Northwest China. Furthermore, Ebrahimy and Azadbakht [33] compared the performance of different ML algorithms in MODIS LST downscaling and concluded RFR performed generally well for such a purpose and outperformed benchmark and other ML algorithms including support vector machines and extreme learning machines.

Although RFR provides promising results in small and/or homogenous areas, its performance over large and heterogeneous areas like Iran may be insufficient because, RFR, as a non-spatial ML algorithm, focuses on the global picture while the level of importance and interaction of different variables in LST downscaling is, most likely, not consistent throughout the entire study area; and it has been well established that the accuracy of a LST downscaling method largely depends on the heterogeneity of the study area and varies across the area of interest [33], [34], [36]. Therefore, development of an individual RFR model for LST downscaling at large scales may not result in an acceptable outcome. To overcome this challenge, this article proposed an adaptive RFR (ARFR) method based on the Köppen climatic zones [37] for LST downscaling at regional and national scales. The main assumption of ARFR is the fact that it is more reasonable to build distinct RFR models for each Köppen climate zone due to the important role of climate status in LST patterns [38]. In fact, utilizing the Köppen climate zones in LST downscaling provides a solid procedure to convert a large heterogeneous area like Iran to several rather homogeneous subsets in terms of the LST variation.

Another challenge for spatiotemporal analysis of downscaled LST at national scale is related to the fact that acquiring, downscaling, and analyzing of a long time-series of MODIS LST product (MOD11A1) are computationally intensive and time-consuming tasks using the conventional software packages. However, with the advent of the cloud computing platforms, such as Google Earth Engine (GEE), this issue has been effectively resolved. GEE is a free big data processing platform to analyze and explore open-access earth observation datasets at multi-petabyte scales [39]–[41]. In fact, combining these massive data sources over 40-years and more than 800 mathematical and spatial functions within GEE facilitates interactive data and algorithm development for a variety of earth observation studies, including those related to spatiotemporal LST trend analyses. Ravanelli *et al.* [42] investigated the potential of the GEE platform for spatiotemporal LST trend monitoring over the period of 1992–2011 and demonstrated the effectiveness of GEE in this regard. Nill *et al.* [43] investigated the influence of different physical surface properties on the LST trends in the summer season using the all available Landsat-5, Landsat-7, and Landsat-8 imageries acquired from 1985 to 2018 within GEE.

Given the above background, this study proposed and implemented an efficient downscaling method (i.e., ARFR) to downscale MODIS LST product. This method was specifically designed for LST downscaling at national scale, as opposed to most of the previous studies that focused on LST downscaling in small scale areas. Moreover, a comprehensive comparison between the RFR algorithm and the proposed method at ten sub-regions was performed to evaluate the robustness of the proposed method. This article also employed GEE for spatiotemporal LST trend analysis in Iran over a long time period using the downscaled MODIS LSTs. In summary, the main objectives of this study are to: develop an efficient downscaling method called ARFR to downscale MODIS LST product from 1-km to 240-m at a national scale; provide an efficient LST downscaling framework to shift from handling single-time image sets to extensive time-series of images within the GEE platform; and determine the spatiotemporal LST trends at both annual and seasonal scales over Iran from 2001 to 2019 with the downscaled daily LST products.

II. Study Area

This study was conducted in Iran which is one the most populated and developed countries in the Middle East, Iran, with an area of about 1 648 195 km^2, is extended from 25° to 40° N, and from 44° to 63° E (see Fig. 1). Most parts of Iran are covered by arid and semi-arid climate with an average annual rainfall of 250 mm [4], [5]. This country is extensively diverse in terms of topography, land cover types, and climate zones [44]. Iran is covered by typical land covers, such as grassland, barren, forest, cropland, built-up, and water bodies.

Ten fixed 80 × 80 km sub-areas (see Fig. 1) covering different land covers, topographies, and climates were also selected to discuss the downscaled LST products in more details. The utilization of such diverse sub-areas led to a robust assessment of the performance of the proposed ARFR method.

III. Materials and Methods

The methodology of this research (see Fig. 2) comprises of five phases, including data collection, data preparation, LST downscaling, accuracy assessment, and spatiotemporal LST analysis. Phase 1 (data collection) consists of acquiring daily MOD11A1 products and different remotely sensed datasets from GEE. Phase 2 (data preparation) includes preprocessing steps, resampling all data to 240-m and 960-m pixel size using the nearest neighbor method, and calculating the Normalized Difference Vegetation Index (NDVI). Phase 3 (LST downscaling) involves model fitting using the proposed ARFR method, implementation of residual correction procedure, and downscaling MODIS LST to 240-m pixel size. Phase 4 (accuracy assessment) includes deriving Landsat-8 LST and calculating standard accuracy metrics by comparison of the retrieved Landsat-8 LST and downscaled LST. Finally, Phase 5 (spatiotemporal LST analysis) comprises of trend analysis of downscaled daily LST data from 2001 to 2019 at both seasonal and annual scales. In this study, phase 1 to 3 and some parts of phase 5 were implemented in the GEE platform. Phase 4 and some other parts of phase 5 were implemented in the R environment. The details of each phase are discussed in the following five subsections.

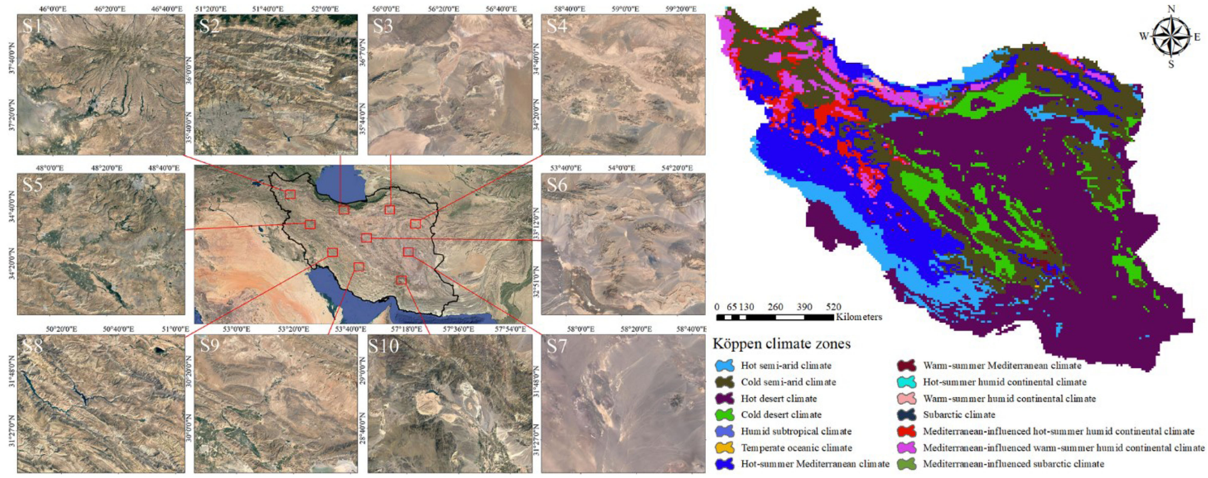

(a) (b)

Fig. 1. (a) Study area (Iran) and ten selected sub-regions which were used for accuracy assessment (background images are RGB color composite of Sentinel-2 images). (b) Spatial distribution of Köppen climate zones in the study area.

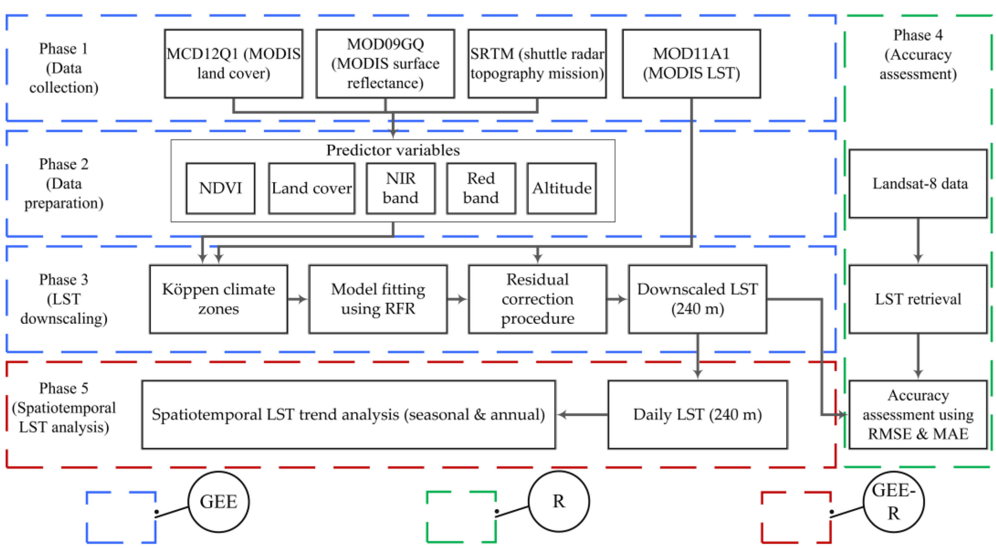

Fig. 2. Flowchart of the proposed method to downscale the MODIS LST products and spatiotemporal LST trend analysis. Colors indicate the platform (GEE) and software (R) which were used in each phase.

A. Phase 1: Data Collection

This article used MODIS daily LST product (MOD11A1) [45], [46], MODIS daily surface reflectance product (MOD09GQ) [47], MODIS yearly land cover product (MCD12Q1) [48], and the Shuttle Radar Topography Mission (SRTM) datasets, which are all available within the GEE data catalog. MOD11A1 is a daily global LST product at the spatial resolution of 1-km, which was retrieved using a split-window algorithm [45], [46], [49]. MOD11A1 product was utilized as the dependent variable. Therefore, in order to account for cloud coverage issue and to improve efficiency of the subsequent analyses, the MOD11A1 products with the available LST pixels of lower than 75% were excluded from datasets. Finally, a total of 3509 MOD11A1 images were accessed and consequently downscaled within the GEE platform for the period of 2001–2019. The MOD09GQ provides the red and near infrared (NIR) spectral bands. The MCD12 which provides global land cover data in 17 classes was accessed within GEE. The SRTM data with 30-m spatial resolution was also retrieved from GEE.

B. Phase 2: Data Preparation

Based on the previous studies [24], [27], [29], [33]–[35], five predictor variables were selected for downscaling MOD11A1 from the pixel size of 1-km to 240-m. Selected predictor variables were the red and NIR bands, NDVI, land cover, and altitude. The red and NIR bands were extracted from the daily MOD09GQ product [47]. The NDVI index was calculated as NDVI = NIR-red / NIR+red. The MCD12Q1 (*the international geosphere-biosphere program classification scheme*) at the spatial resolution of 500-m [48] was used as the land cover data. Finally, the altitude information was derived from the SRTM dataset. All the predictor variables were resampled to pixel sizes of 960-m and 240-m to be used in model fitting and LST downscaling, respectively. The rationale for using the pixel sizes of 960-m and 240-m was that these values correspond to integer multipliers of the spatial resolution of the SRTM and Landsat-8 datasets and also close to the source data's native resolution [34], [46].

C. Phase 3: LST Downscaling

The basis of the proposed LST downscaling method was the RFR method and, thus, it is first discussed. RFR, as an ensemble and highly advanced ML method, uses bootstrap resampling method to create a large number of random decision trees [50]. By using the bootstrap method, each tree trains on a random subset with replacement of the entire training dataset [50], [51]. RFR is known as an effective ML method not only for its good prediction accuracy, but also for its great ability to deal with nonlinear and complex real world problems [52], [53].The key initiative of RFR is the combination of a collection of decision trees and selection of a subset of explanatory variables at individual trees. Subsequently, each of the built decision trees provides an individual value, and then the algorithm considers the average value as the final prediction in regression tasks. Two meta-parameters should be adjusted to obtain an optimal RFR model: the number of decision trees in the forest (*ntree*) and the number of predictor variables randomly selected on each node of the trees (*mtry*). According to Belgiu and Drăguţ [53] and the preliminary analyses in this article (e.g., trial and errors), the values of *ntree* and *mtry* were set to 500 and 2, respectively.

The main assumption in development of the proposed ARFR method is that the characteristics of LST values is different at various climatic zones. Consequently, building specific RFR model for each Köppen climate zone can lead to a more accurate LST downscaling outcome. Accordingly, to implement ARFR, the whole study area was first masked by each Köppen climate zone and a specific RFR was developed for each zone. For each Köppen climate zone, the LST downscaling procedure was conducted in three stages: First, the relationship between the MOD11A1 LST product and the predictor variables was established for the 960-m datasets using the RFR method. Second, the developed RFR model was applied to the predictor variables on the 240-m datasets to predict downscaled LST at pixel size of 240-m. Third, a residual correction process [54] was adopted to the LST downscaling procedure. To this end, a pixel-wise residual between the predicted LST and original MODIS LST for 960-m was first calculated. Then, the 960-m residual was resampled to 240-m and was finally added to the downscaled LST map. Finally, once this procedure was completed for all Köppen climate zones, the results were mosaicked to produce the final downscaled LST map.

D. Phase 4: Accuracy Assessment

Landsat-8 thermal imageries acquired at different dates of six consecutive years (2014–2019) were employed for the accuracy assessment of the downscaled LST maps. Six Landsat-8 scenes were processed for each sub-area (See Fig. 1). In total, 60 Landsat-8 images were used for accuracy assessment purposes.

The LST of Landsat-8 thermal images was retrieved in accordance with the proposed method by Duan *et al*. [55], using a single-channel method. Additionally, because of the structural differences of the MODIS and Landsat-8 sensors, direct comparison between the downscaled and the reference Landsat-8 LSTs is not reasonable [25], [34]. Therefore, to convert the Landsat-8 LST to its MODIS LST equivalent, inter-sensor conversion coefficients were derived using linear regression between aggregated Landsat-8 LST and MODIS LST at 960-m according to the proposed method by Bindhu *et al*. [25]. Then, these coefficients were applied to 240-m Landsat LSTs.

Finally, the root mean sqaure error (RMSE) and the mean absolute error (MAE), as two widely adopted evaluation metrics in LST downscaling studies [24], were computed to evaluate the accuracy of downscaled LSTs. The conventional RFR method was also implemented to determine the reliability of ARFR in comparison to the RFR methods.

E. Phase 5: LST Trend Analysis

LST trend analysis describes fluctuations of the LST values of a given location over a specific period of time. A variety of different experiments were accomplished to investigate both seasonal and annual spatiotemporal variability of LST over Iran, and its trends from 2001 to 2019 using the downscaled daily LSTs at the pixel size of 240-m. To this end, per-pixel magnitude of annual changes in LST values were first investigated by comparing LST values across time series. Then, in order to define the extent of changes in LST at pixel level, the Theil–Sen slope [56], [57] of the LST trend was used as an indicator of the extent of changes in LST per season/year, where positive (negative) values indicate an upward (downward) or increasing (decreasing) trend.

Moreover, for both seasonal and annual series of LST, the per-pixel significance of trends was calculated at the 95% confidence level. In this regard, the nonparametric Mann–Kendall test [58], [59] was applied to LST time series due to the possible effects of temporal autocorrelation on estimated significance of trends. Finally, the LST time-series data were used to assess temporal variability of LST across Iran in different seasons. The seasons were defined in the standard climatological routine: spring defined as March to May, summer as June to August, fall as September to November, and winter as December to February.

IV. Results and Discussion

In this part, after providing a comprehensive accuracy assessment of the ARFR method in LST downscaling in Section IV-A, the results of the overall, spatial and temporal trend analyses are presented in Section IV-B.

A. LST Downscaling Using the Proposed ARFR Method

In this section, first the visual comparison of the downscaled LST maps with original MODIS LST product and Landsat-8

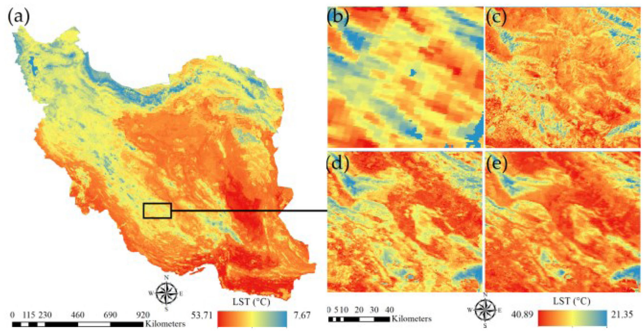

Fig. 3. Visual comparison of the downscaled LST maps with the original MOD11A1 and Landsat-8 LST for the acquired image on 02/10/2018. (a) Downscaled MOD11A1 of Iran using ARFR with 240-m pixel size; (b) MOD11A1 with 960-m pixel size of *S*9. (c) Landsat-8 with 240-m pixel size of S9. (d) Downscaled MOD11A1 using ARFR with 240-m pixel size of *S*9, (e) Downscaled MOD11A1 using RFR with 240-m pixel size of *S*9.

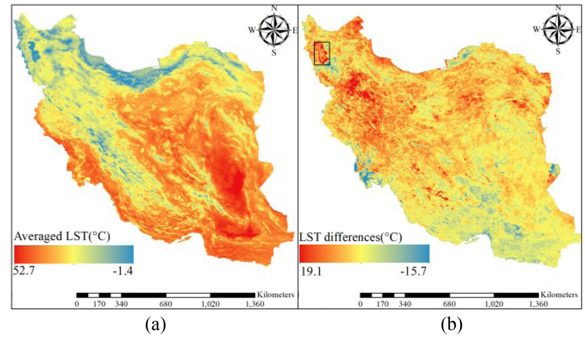

Fig. 4. (a) Spatial distribution of averaged LST over 2001–2019 and (b) LST differences between 2001 and 2019. The black rectangle in (b) indicates the Urmia lake.

LST data is presented. The accuracy assessment results over ten different sub-areas are then provided.

To visually evaluate the downscaled LST maps, the visual comparison of the downscaled LST maps using ARFR and RFR with the original MODIS LST and the Landsat-8 reference LST in S9 for 02/10/2018 is presented in Fig. 3. Although the downscaled LST maps with ARFR and RFR provided similar spatial distribution with those of the MODIS and Landsat-8 LST data, ARFR provided much more details than RFR. As shown in Fig. 3, ARFR not only retrieved much of the LST variation visible in the Landsat-8 LST map, but also substantially improved visual information in comparison to the original MOD11A1 image. On the other hand, RFR provided less details in comparison to ARFR and tended to overestimate the LST values.

The calculated accuracy indicators (i.e., RMSE and MAE) for the selected sub-areas (see Fig. 1) on different dates are given in Table I. The results demonstrated the robustness and the better performance of the proposed ARFR method with an average RMSE of 2.22 °C and MAE of 1.59 °C in comparison to RFR with an average RMSE of 3.13 °C and MAE of 2.51 °C. The RMSE and MAE values on different dates obtained from ARFR varied from 1.1 °C to 3.86 °C and from 0.61 °C to 2.77 °C, respectively. On the other hand, RMSE and MAE values of RFR were in the range of 1.34 to 4.94 °C and 1.03 to 3.9 °C, respectively.

On average, the highest accuracies of ARFR among the selected sub-areas were obtained for S5 (RMSE = 1.52 °C, MAE = 0.91 °C) and S9 (RMSE = 1.88 °C, MAE = 1.28 °C), while the lowest accuracies were observed for S2 (RMSE = 3.45 °C, MAE = 2.6 °C) and S10 (RMSE = 2.91 °C, MAE = 1.95 °C). A possible reason for the errors might be related to the potential uncertainties in the developed ARFR and RFR models associated with input data, as well as the primary accuracy level of the MODIS LST product which was reported to be approximately 1 °C –2 °C [45], [49], [60]. Moreover, several studies [61], [62] reported that the MODIS LST product showed noticeable uncertainties in the regions covered by barren land.

With regards to the RMSE and MAE values, performance of the downscaling procedure was in agreement with other studies which attempted to downscale MODIS LST using RFR [33]–[35]. In summary, it can be concluded that the ARFR method had satisfactory performance in LST downscaling in different settings. Therefore, the downscaled LST maps with ARFR can be used in spatiotemporal LST trend analysis over Iran.

Although ARFR provide good performance in MODIS LST downscaling at national scale, the suitability of the proposed ARFR method for different satellite imageries across different spatial scales ranging from continental to global should be investigated in future studies. Finally, it is worth noting that the accuracy of LST downscaling could be decreased by increasing the heterogeneity or complexity of a given area [33], [34], [36]. Thus, it is recommended to investigate the impact of heterogeneity on the accuracy of downscaled LST products using the ARFR method in the future studies.

B. Spatiotemporal LST Trend

This section comprises three subsections. Subsection IV-B-1 is presented to investigate the overall LST trend over the examined period. The succeeding subsection IV-B-2 and subsection IV-B-3 are provided to further discuss the spatial and temporal LST trends.

1) Overall LST Trends: The downscaled daily LSTs from 2001 to 2019 were used to estimate both seasonal and annual spatiotemporal trends of LST. The annually averaged LST during the period of 2001–2019 is represented in Fig. 4(a). Based on the results, the LST varied from -1.4 °C to 52.7 °C over Iran, with a mean value of 35.4 °C. The LST values increased from northwest to southeast.

In order to determine the overall magnitude of changes, the mean annual LST of 2019 was subtracted from that of 2001, and the results are illustrated in Fig. 4(b). An increasing trend was observed in most parts of the study area, while minor parts experienced a decreasing trend. Nevertheless, a general increase in LST is the main pattern in Iran, which has also been reported in other studies [5], [6]. The highest increasing trends were observed in areas covered with barren, cropland, and residential areas. This pattern can be attributed to urban growth, climate change, human activities, and potential changes in farming systems during the examined period.

2) Spatial LST Trends: To provide an analytical explanation for the spatial LST trends, both the slope and *p*-values of the

TABLE I
RMSE (MAE) Values of the Selected Subareas on Different Dates Using ARFR and RFR Methods

S1			S2			S3		
Date	ARFR	RFR	Date	ARFR	RFR	Date	ARFR	RFR
14/08/2014	1.50 (0.88)	1.94 (1.51)	08/12/2014	3.44 (2.73)	4.19 (3.30)	09/05/2014	2.45 (1.72)	3.57 (2.84)
17/08/2015	2.38 (1.76)	3.53 (3.01)	24/10/2015	3.43 (2.66)	4.80 (3.78)	19/10/2015	1.80 (1.28)	2.20 (1.71)
06/10/2016	1.56 (1.01)	2.42 (2.27)	23/08/2016	3.86 (2.80)	4.61 (3.47)	05/10/2016	1.73 (1.26)	2.13 (1.78)
22/08/2017	1.81 (1.30)	2.59 (2.49)	26/08/2017	3.09 (2.10)	4.10 (3.18)	21/08/2017	1.83 (1.29)	3.12 (2.50)
25/08/2018	1.10 (0.61)	2.61 (1.05)	29/08/2018	3.32 (2.54)	4.46 (3.66)	24/08/2018	1.86 (1.31)	2.74 (2.27)
15/10/2019	1.80 (1.20)	1.34 (1.03)	03/10/2019	3.60 (2.77)	4.64 (3.76)	27/08/2019	1.97 (1.60)	2.38 (2.07)
Average	1.69 (1.13)	2.41 (1.89)	Average	3.46 (2.60)	4.47 (3.53)	Average	1.94 (1.41)	2.69 (2.20)
S4			S5			S6		
Date	ARFR	RFR	Date	ARFR	RFR	Date	ARFR	RFR
31/08/2014	2.60 (1.98)	2.85 (2.33)	17/09/2014	1.62 (0.88)	2.37 (1.70)	26/12/2014	1.95 (1.33)	2.60 (1.98)
05/10/2015	2.70 (2.08)	3.16 (2.72)	19/08/2015	1.60 (1.05)	2.04 (1.57)	10/10/2015	2.37 (1.82)	3.31 (2.74)
21/09/2016	2.10 (1.54)	2.47 (2.03)	05/08/2016	1.32 (0.72)	1.72 (1.29)	25/08/2016	3.21 (2.74)	4.14 (3.75)
24/09/2017	1.80 (1.18)	2.28 (1.83)	25/09/2017	1.45 (0.89)	2.03 (1.59)	31/10/2017	1.52 (0.99)	2.37 (1.83)
27/09/2018	1.78 (1.07)	2.78 (2.19)	27/08/2018	1.43 (0.99)	2.19 (1.78)	02/10/2018	1.81 (1.51)	2.25 (1.76)
16/10/2019	1.87 (1.28)	2.38 (2.05)	01/10/2019	1.69 (0.94)	2.38 (1.66)	24/12/2019	1.76 (1.09)	2.73 (2.22)
Average	2.14 (1.52)	2.65 (2.19)	Average	1.52 (0.91)	2.12 (1.60)	Average	2.10 (1.58)	2.90 (2.38)
S7			S8			S9		
Date	ARFR	RFR	Date	ARFR	RFR	Date	ARFR	RFR
31/08/2014	2.08 (1.62)	3.88 (3.49)	19/09/2014	2.38 (1.71)	3.11 (2.41)	04/08/2014	1.81 (1.18)	2.51 (1.94)
18/08/2015	2.92 (2.33)	3.60 (3.18)	21/08/2015	2.69 (1.91)	3.57 (2.79)	26/10/2015	2.41 (1.68)	3.39 (2.75)
20/08/2016	1.87 (1.77)	2.82 (2.79)	23/08/2016	2.46 (1.69)	3.71 (2.87)	09/08/2016	1.94 (1.33)	2.74 (2.13)
26/10/2017	1.44 (1.26)	2.94 (2.87)	29/10/2017	2.39 (1.62)	3.66 (2.83)	28/08/2017	1.72 (1.19)	2.47 (1.92)
26/08/2018	2.17 (1.96)	3.59 (3.54)	13/08/2018	2.09 (1.40)	3.20 (2.45)	02/10/2018	1.40 (0.91)	2.28 (1.75)
16/10/2019	2.18 (2.01)	3.69 (3.62)	03/10/2019	2.52 (1.58)	3.52 (2.46)	05/10/2019	2.01 (1.41)	2.41 (1.85)
Average	2.11 (1.83)	3.42 (3.25)	Average	2.42 (1.65)	3.46 (2.64)	Average	1.88 (1.28)	2.63 (2.06)
S10								
Date	ARFR	RFR						
18/10/2014	3.72 (2.57)	4.62 (3.25)						
18/08/2015	3.10 (2.01)	4.75 (3.63)						
23/10/2016	2.79 (1.93)	4.93 (3.90)						
26/10/2017	2.64 (1.82)	4.63 (3.49)						
26/08/2018	2.19 (1.32)	4.94 (3.70)						
30/09/2019	3.03 (2.07)	3.27 (2.42)						
Average	2.91 (1.95)	4.52 (3.40)						

LST trend over time were calculated based on the annual time steps from both annually and seasonally aggregated values of the entire interval (2001–2019) (see Fig. 5). For this purpose, the slopes and *p*-values were classified into four classes as follows:

1) SNT: Significant negative trend (slope < 0 and p-value ≤ 0.05).

2) NSNT: Nonsignificant negative trend (slope < 0 and p-value > 0.05).

3) NSPT: Nonsignificant positive trend (slope > 0 and p-value > 0.05).

4) SPT: Significant positive trend (slope > 0 and p-value ≤ 0.05).

The analysis of the results indicated multiple strong inconsistencies in inter-seasonal trends as well as between annual and seasonal trends over time. At the annual scale, most parts of the study area (57.67%) were associated with NSPT and SPT classes. Approximately 39% of the study area was covered by NSNT class, mostly in the southern parts of the region. Moreover, 3.09% of the areas exhibited the SNT class. This showed that the overall LST trend was incremental through the studied period and the areas with significant trends (either negative or positive) were mostly related to the barren, agricultural and residential areas, respectively.

At the seasonal scales, the variability of the defined classes at different seasons was rather complex. In spring, for example, 33.89% of the study area represented a significant trend, most of which were related to the SNT class that were spatially incomparable with the annual trends. In the summer season, the SPT class covered most parts of the study area (56.68%), while the SNT and NSNT classes covered 7.54% and 12.87% of the study area, respectively. Similar to spring season and in contrast to other seasons, inspection of the results in fall indicated a decreasing LST trend. In this season, the NSNT (63.53%) and SNT (17.38%) classes dominated a large portion of the country. Finally, in the winter season, approximately 58% of the region experienced increasing LST trend, a part of which (32.84%) corresponded to the SPT class. By investigating the results of the fall and winter seasons, it was observed that these seasons were affected by LST variability the most. These results were reasonable due to the potential impacts of the climate change (e.g., temperature anomalies, extreme weather events, and drought) and shifting in seasons, which usually leads to lower LST values in fall (the earlier emergence of winter) and higher LST values in winter (the earlier emergence of spring).

As an example, the Urmia Lake located in the northwest part of Iran experienced a substantial warning trend (see Fig. 4). The rate of the LST change over this lake from 2001 to 2019 was remarkably high, especially along the shallow shoreline areas. The LST of shallow shoreline areas increased by around 10 °C, while the LST of the central areas of this lake increased approximately by 3 °C. Moreover, based on the LST trend classes (see Fig. 5), the Urmia Lake was covered by SPT class in both

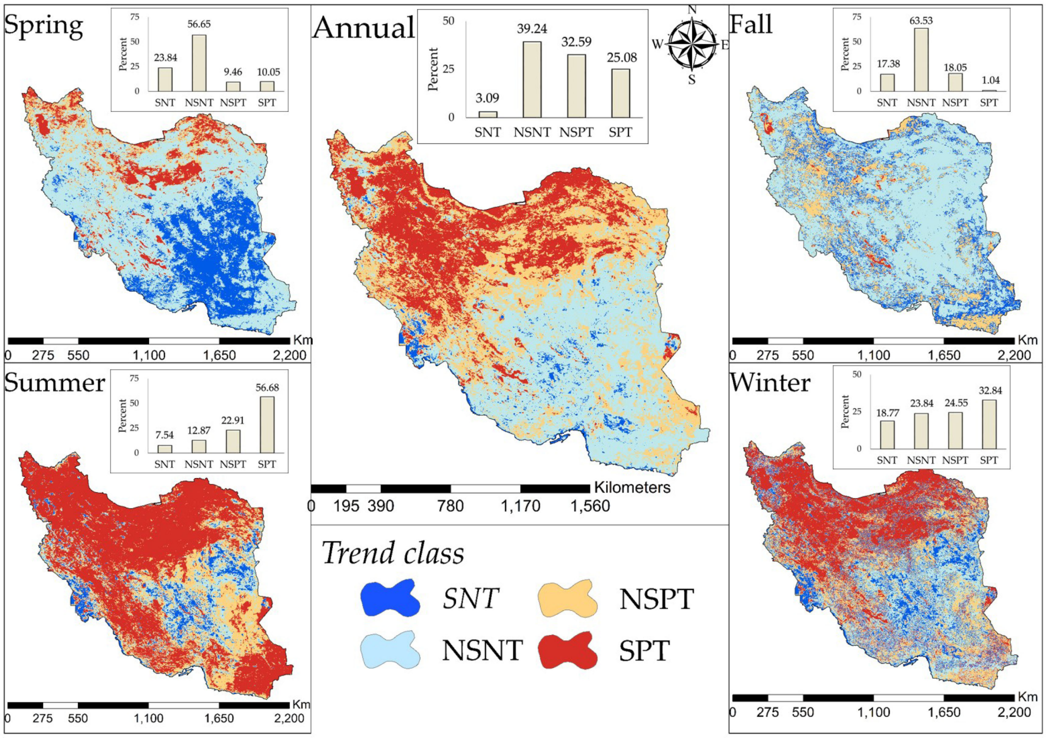

Fig. 5. Spatial and statistical patterns of the LST trend classes at annual and seasonal scales. SNT: slope < 0 and p-value ≤ 0.05; NSNT: slope < 0 and p-value > 0.05; NSPT: slope > 0 and p-value > 0.05; and SPT: slope > 0 and p-value ≤ 0.05.

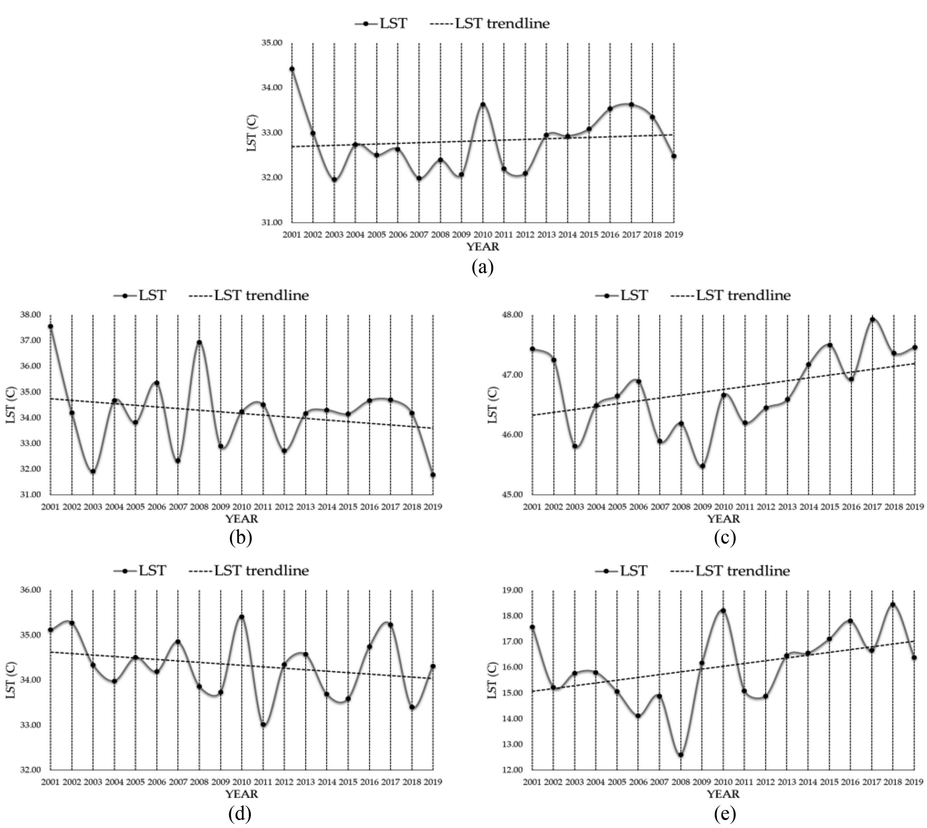

Fig. 6. Temporal variations of the (a) annual and (b)–(e) seasonal (i.e., spring, summer, fall, and winter, respectively) averaged LST of Iran over 2001–2019.

annual and seasonal scales. This was reasonable given the fact that this area was experienced a severe drought period in recent decades, mainly because of the climate change impacts and human activities (e.g., agricultural water management activities) [63].

In summary, spatial representation of LST changes showed an uneven distribution mostly related to the heterogeneity of the study area, in which it was difficult to precisely interpret LST trends that need to be further investigated in order to analyze other potential causes. Additionally, since this study demonstrated the complexity and variability of the spatiotemporal LST trends in both annual and seasonal scales, it would be worthwhile to thoroughly investigate what factors influence these trends and whether these influences are constant over time in future studies.

3) Temporal LST Trends: Temporal variability of LST was investigated by seasonally averaged LST values over the entire period, and the results are demonstrated in Fig. 6. Seasonal LST trends, apart from fall and spring, showed fairly increasing trends (see Fig. 6), which was in agreement with the annual trend. Spring and winter showed larger variations in the LST values compared to summer and fall. The LST values in spring, summer, fall, and winter varied between 31.8 °C –37.6 °C, 45.8 °C – 47.9 °C, 33 °C –35 °C, and 12.6 °C –18.4 °C, respectively. The highest LST values were observed in summer of 2017 and 2015, reaching up to 47.9 °C and 47.5 °C, respectively. The lowest LST values were observed in winter of 2008 and 2006, reaching down to 12.6 °C and 14.1 °C, respectively. Based on the results, substantial LST variations between different years were observed in all the seasons. As an example, in spring, a sharp increase was observed from 32.3 °C in 2007 to 36.9 °C in 2008 and thereafter a sharp drop was observed to 32.9 °C in 2009. The significant variation might be related to the fact that the adopted approach computed only one average for all downscaled LST values in each season of a given year, which in turn, reduced the possibility of comprehensive trend analysis. Therefore, in future studies and in order to analyze LST trends more specifically, it is necessary to use daily downscaled LST and local models simultaneously.

V. Conclusion

This article investigated the spatiotemporal LST trends at both annual and seasonal scales during the period of 2001–2019 over Iran using a proposed downscaling algorithm, called ARFR. ARFR was developed using RFR and based on Köppen climate zones to downscale MODIS LST products (MOD11A1) in both spatial (240-m pixel size) and temporal (daily) resolutions. The results of this article demonstrated that the application of ARFR within the GEE platform was efficient to downscale MOD11A1 in terms of accuracy (average RMSE of 2.22 °C and MAE of 1.59 °C) and computational performance. Furthermore, the downscaled daily LST maps at 240-m pixel size were used to investigate spatiotemporal LST trends in Iran. In general, although an increasing trend of LST with uneven spatial pattern was observed in the study area except for fall season, variability of the LST trends indicated inconsistencies in inter-seasonal trends as well as between annual and seasonal trends over the examined period. The results of spatiotemporal analysis of daily LST trends over 19 years would be useful for better understanding climate change and land processes. In summary, the results of this study suggest that the proposed downscaling method along with the freely available datasets within GEE platform can be beneficial for studies related to spatiotemporal LST trend analysis and climate change.

References

[1] "Climate change 2013—the physical science basis: Working group I contribution to the fifth assessment report of the intergovernmental panel on climate change," *Intergovern. Panel Climate Change*, Geneva, Switzerland, 2014.

[2] D. Eleftheriou *et al.*, "Determination of annual and seasonal daytime and nighttime trends of MODIS LST over Greece—climate change implications," *Sci. Total Environ.*, vol. 616-617, pp. 937–947, 2018.

[3] M. Khorchani *et al.*, "Trends in LST over the peninsular Spain as derived from the AVHRR imagery data," *Global Planetary Change*, vol. 166, pp. 75–93, 2018.

[4] M. Amani, B. Salehi, S. Mahdavi, A. Masjedi, and S. Dehnavi, "Temperature-vegetation-soil moisture dryness index (TVMDI)," *Remote Sens. Environ.*, vol. 197, pp. 1–14, 2017.

[5] A. R. Ghasemi, "Changes and trends in maximum, minimum and mean temperature series in Iran," *Atmos. Sci. Let.*, vol. 16, no. 3, pp. 366–372, 2015.

[6] H. Tabari and P. Hosseinzadeh Talaee, "Analysis of trends in temperature data in arid and semi-arid regions of Iran," *Global Planetary Change*, vol. 79, no. 1, pp. 1–10, 2011.

[7] Z.-L. Li *et al.*, "Satellite-derived land surface temperature: Current status and perspectives," *Remote Sens. Environ.*, vol. 131, pp. 14–37, 2013.

[8] R. Van De Kerchove, S. Lhermitte, S. Veraverbeke, and R. Goossens, "Spatio-temporal variability in remotely sensed land surface temperature, and its relationship with physiographic variables in the Russian Altay mountains," *Int. J. Appl. Earth Observ. Geoinf.*, vol. 20, pp. 4–19, 2013.

[9] Y. Julien, J. A. Sobrino, and W. Verhoef, "Changes in land surface temperatures and NDVI values over Europe between 1982 and 1999," *Remote Sens. Environ.*, vol. 103, no. 1, pp. 43–55, 2006.

[10] I. Sandholt, K. Rasmussen, and J. Andersen, "A simple interpretation of the surface temperature/vegetation index space for assessment of surface moisture status," *Remote Sens. Environ.*, vol. 79, no. 2, pp. 213–224, 2002.

[11] P. Sismanidis, I. Keramitsoglou, C. Kiranoudis, and B. Bechtel, "Assessing the capability of a downscaled urban land surface temperature time series to reproduce the spatiotemporal features of the original data," *Remote Sens.*, vol. 8, no. 4, 2016, Art. no. 274.

[12] M. C. Anderson, J. M. Norman, W. P. Kustas, R. Houborg, P. J. Starks, and N. Agam, "A thermal-based remote sensing technique for routine mapping of land-surface carbon, water and energy fluxes from field to regional scales," *Remote Sens. Environ.*, vol. 112, no. 12, pp. 4227–4241, 2008.

[13] W. Kustas and M. Anderson, "Advances in thermal infrared remote sensing for land surface modeling," *Agricultural Forest. Meteorol.*, vol. 149, no. 12, pp. 2071–2081, 2009.

[14] J. Muro *et al.*, "Land surface temperature trends as indicator of land use changes in wetlands," *Int. J. Appl. Earth Observ. Geoinf.*, vol. 70, pp. 62–71, 2018.

[15] Q. Weng, D. Lu, and J. Schubring, "Estimation of land surface temperature–vegetation abundance relationship for urban heat island studies," *Remote Sens. Environ.*, vol. 89, no. 4, pp. 467–483, 2004.

[16] P. Fu and Q. Weng, "Variability in annual temperature cycle in the urban areas of the united states as revealed by MODIS imagery," *ISPRS J. Photogramm. Remote Sens.*, vol. 146, pp. 65–73, 2018.

[17] Q. Weng, "Thermal infrared remote sensing for urban climate and environmental studies: Methods, applications, and trends," *ISPRS J. Photogramm. Remote Sens.*, vol. 64, no. 4, pp. 335–344, 2009.

[18] N. T. Son, C. F. Chen, C. R. Chen, L. Y. Chang, and V. Q. Minh, "Monitoring agricultural drought in the lower mekong basin using MODIS NDVI and land surface temperature data," *Int. J. Appl. Earth Observ. Geoinf.*, vol. 18, pp. 417–427, 2012.

[19] M. Langer, S. Westermann, and J. Boike, "Spatial and temporal variations of summer surface temperatures of wet polygonal tundra in Siberia - implications for MODIS LST based permafrost monitoring," *Remote Sens. Environ.*, vol. 114, no. 9, pp. 2059–2069, 2010.

[20] N. Nandkeolyar and G. Sandhya Kiran, "A climatological study of the spatio-temporal variability of land surface temperature and vegetation cover of Vadodara district of Gujarat using satellite data," *Int. J. Remote Sens.*, vol. 40, pp. 218–236, 2019.

[21] P. Sismanidis, B. Bechtel, I. Keramitsoglou, and C. T. Kiranoudis, "Mapping the spatiotemporal dynamics of Europe's land surface temperatures," *IEEE Geosci. Remote Sens. Lett.*, vol. 15, no. 2, pp. 202–206, Feb. 2018.

[22] W. Ha, P. H. Gowda, and T. A. Howell, "Downscaling of land surface temperature maps in the Texas high plains with the TsHARP method," *GISci. Remote Sens.*, vol. 48, no. 4, pp. 583–599, 2011.

[23] Y. Jiang and Q. Weng, "Estimation of hourly and daily evapotranspiration and soil moisture using downscaled LST over various urban surfaces," *GISci. Remote Sens.*, vol. 54, no. 1, pp. 95–117, 2017.

[24] W. Zhan *et al.*, "Disaggregation of remotely sensed land surface temperature: Literature survey, taxonomy, issues, and caveats," *Remote Sens. Environ.*, vol. 131, pp. 119–139, 2013.

[25] V. M. Bindhu, B. Narasimhan, and K. P. Sudheer, "Development and verification of a non-linear disaggregation method (NL-DisTrad) to downscale MODIS land surface temperature to the spatial scale of landsat thermal data to estimate evapotranspiration," *Remote Sens. Environ.*, vol. 135, pp. 118–129, 2013.

[26] S. Duan and Z. Li, "Spatial downscaling of MODIS land surface temperatures using geographically weighted regression: Case study in Northern China," *IEEE Trans. Geosci. Remote Sens.*, vol. 54, no. 11, pp. 6458–6469, Nov. 2016.

[27] F. Gao, W. Kustas, and M. Anderson, "A data mining approach for sharpening thermal satellite imagery over land," *Remote Sens*, vol. 4, no. 11, pp. 3287–3319, 2012.

[28] W. Li, L. Ni, Z. Li, S. Duan, and H. Wu, "Evaluation of machine learning algorithms in spatial downscaling of MODIS land surface temperature," *IEEE J. Sel. Top. Appl. Earth Obs. Remote Sens.*, vol. 12, no. 7, pp. 2299–2307, Jul. 2019.

[29] K. Zakšek and K. Oštir, "Downscaling land surface temperature for urban heat island diurnal cycle analysis," *Remote Sens. Environ.*, vol. 117, pp. 114–124, 2012.

[30] D. Liu and X. Zhu, "An enhanced physical method for downscaling thermal infrared radiance," *IEEE Geosci. Remote Sens. Lett.*, vol. 9, no. 4, pp. 690–694, Jul. 2012.

[31] Q. Weng, P. Fu, and F. Gao, "Generating daily land surface temperature at Landsat resolution by fusing landsat and MODIS data," *Remote Sens. Environ.*, vol. 145, pp. 55–67, 2014.

[32] P. Wu, H. Shen, L. Zhang, and F.-M. Göttsche, "Integrated fusion of multi-scale polar-orbiting and geostationary satellite observations for the mapping of high spatial and temporal resolution land surface temperature," *Remote Sens. Environ.*, vol. 156, pp. 169–181, 2015.

[33] H. Ebrahimy and M. Azadbakht, "Downscaling MODIS land surface temperature over a heterogeneous area: An investigation of machine learning techniques, feature selection, and impacts of mixed pixels," *Comput. Geosci.*, vol. 124, pp. 93–102, 2019.

[34] C. Hutengs and M. Vohland, "Downscaling land surface temperatures at regional scales with random forest regression," *Remote Sens. Environ.*, vol. 178, pp. 127–141, 2016.

[35] Y. Yang, C. Cao, X. Pan, X. Li, and X. Zhu, "Downscaling land surface temperature in an arid area by using multiple remote sensing indices with random forest regression," *Remote Sens*, vol. 9, no. 8, 2017, Art. no. 789.

[36] S. Mukherjee, P. K. Joshi, and R. D. Garg, "A comparison of different regression models for downscaling Landsat and MODIS land surface temperature images over heterogeneous landscape," *Adv. Space Res.*, vol. 54, no. 4, pp. 655–669, 2014.

[37] M. C. Peel, B. L. Finlayson, and T. A. McMahon, "Updated world map of the Köppen-Geiger climate classification," *Hydrol. Earth Syst. Sci.*, vol. 11, no. 5, pp. 1633–1644, 2007.

[38] C. Wang, Y. Li, S. W. Myint, Q. Zhao, and E. A. Wentz, "Impacts of spatial clustering of urban land cover on land surface temperature across Köppen climate zones in the contiguous United States," *Landscape Urban Planning*, vol. 192, 2019, Art. no. 103668.

[39] M. Amani *et al.*, "Google Earth Engine cloud computing platform for remote sensing big data applications: A comprehensive review," *IEEE J. Sel. Top. Appl. Earth Observ. Remote Sens.*, vol. 13, pp. 5326–5350, 2020.

[40] M. Amani *et al.*, "Canadian wetland inventory using Google Earth Engine: The first map and preliminary results," *Remote Sens*, vol. 11, no. 7, 2019, Art. no. 842.

[41] N. Gorelick, M. Hancher, M. Dixon, S. Ilyushchenko, D. Thau, and R. Moore, "Google Earth Engine: Planetary-scale geospatial analysis for everyone," *Remote Sens. Environ.*, vol. 202, pp. 18–27, 2017.

[42] R. Ravanelli *et al.*, "Monitoring the impact of land cover change on surface urban heat island through Google Earth Engine: Proposal of a global methodology, first applications and problems," *Remote Sens*., vol. 10, no. 9, 2018, Art. no. 1488.

[43] L. Nill, T. Ullmann, C. Kneisel, J. Sobiech-Wolf, and R. Baumhauer, "Assessing spatiotemporal variations of landsat land surface temperature and multispectral indices in the Arctic Mackenzie delta region between 1985 and 2018," *Remote Sens*, vol. 11, no. 19, 2019, Art. no. 2329.

[44] A. Shahabfar, A. Ghulam, and J. Eitzinger, "Drought monitoring in Iran using the perpendicular drought indices," *Int. J. Appl. Earth Observ. Geoinf.*, vol. 18, pp. 119–127, 2012.

[45] Z. Wan, "New refinements and validation of the collection-6 MODIS land-surface temperature/emissivity product," *Remote Sens. Environ.*, vol. 140, pp. 36–45, 2014.

[46] Z. Wan, S. Hook, and G. Hulley, "MOD11A1 MODIS/terra land surface temperature/emissivity daily L3 global 1km SIN grid V006 [Data set. NASA EOSDIS LP DAAC," 2015.

[47] E. Vermote and R. Wolfe, "MOD09GQ: MODIS/Terra surface reflectance daily L2G global 250m SIN grid V006," 2015. Accessed: Sep. 25, 2018. [Online]. Available [online]: https://lpdaac.usgs.gov/dataset_discovery/modis/modis_products_table/mod09gq_v006

[48] M. A. Friedl *et al.*, "MODIS collection 5 global land cover: Algorithm refinements and characterization of new datasets," *Remote Sens. Environ.*, vol. 114, no. 1, pp. 168–182, 2010.

[49] S.-B. Duan *et al.*, "Validation of collection 6 MODIS land surface temperature product using in situ measurements," *Remote Sens. Environ.*, vol. 225, pp. 16–29, 2019.

[50] L. Breiman, "Random forests," *Mach. Learn.*, vol. 45, no. 1, pp. 5–32, 2001.

[51] A. Liaw and M. Wiener, "Classification and regression by randomForest," *R News*, vol. 2, no. 3, pp. 18–22, 2002.

[52] M. Azadbakht, C. S. Fraser, and K. Khoshelham, "Synergy of sampling techniques and ensemble classifiers for classification of urban environments using full-waveform LiDAR data," *Int. J. Appl. Earth Observ. Geoinf.*, vol. 73, pp. 277–291, 2018.

[53] M. Belgiu and L. Drăguţ, "Random forest in remote sensing: A review of applications and future directions," *ISPRS J. Photogramm. Remote Sens.*, vol. 114, pp. 24–31, 2016.

[54] C. Jeganathan, N. A. S. Hamm, S. Mukherjee, P. M. Atkinson, P. L. N. Raju, and V. K. Dadhwal, "Evaluating a thermal image sharpening model over a mixed agricultural landscape in India," *Int. J. Appl. Earth Observ. Geoinf.*, vol. 13, no. 2, pp. 178–191, 2011.

[55] S.-B. Duan *et al.*, "Land-surface temperature retrieval from Landsat 8 single-channel thermal infrared data in combination with NCEP reanalysis data and ASTER GED product," *Int. J. Remote Sens.*, vol. 40, no. 5-6, pp. 1763–1778, 2019.

[56] P. K. Sen, "Estimates of the regression coefficient based on Kendall's Tau," *J. Amer. Statist. Assoc.*, vol. 63, no. 324, pp. 1379–1389, 1968.

[57] H. Theil, "A rank-invariant method of linear and polynomial regression analysis," in *Henri Theil's Contributions to Economics and Econometrics: Econometric Theory and Methodology*. B. Raj and J. Koerts Eds.. Dordrecht, The Netherlands: Springer, 1992, pp. 345–381.

[58] M. G. Kendall, *Rank Correlation Methods*. London, U.K.: Griffin, 1975.

[59] H. B. Mann, "Nonparametric tests against trend," *Econometrica*, vol. 13, no. 3, pp. 245–259, 1945.

[60] S.-B. Duan, Z.-L. Li, H. Wu, P. Leng, M. Gao, and C. Wang, "Radiance-based validation of land surface temperature products derived from collection 6 MODIS thermal infrared data," *Int. J. Appl. Earth Observ. Geoinf.*, vol. 70, pp. 84–92, 2018.

[61] H. Li *et al.*, "Temperature-based and radiance-based validation of the collection 6 MYD11 and MYD21 land surface temperature products over barren surfaces in northwestern China," *IEEE Trans. Geosci. Remote Sens.*, vol. 59, no. 2, pp. 1794–1807, Feb. 2021.

[62] H. Li *et al.*, "Temperature-based and radiance-based validation of the collection 6 MYD11 and MYD21 land surface temperature products over barren surfaces in northwestern China," *IEEE Trans. Geosci. Remote Sens.*, vol. 59, no. 2, pp. 1794–1807, Feb. 2021.

[63] A. H. Delju, A. Ceylan, E. Piguet, and M. Rebetez, "Observed climate variability and change in Urmia lake basin, Iran," *Theor. Appl. Climatol.*, vol. 111, no. 1, pp. 285–296, 2013.

Hamid Ebrahimy received the M.S. degree in remote sensing and GIS from University of Tabriz, Tabriz, Iran, in 2016.

He is currently a Researcher with Center for Remote Sensing and GIS Research, Shahid Beheshti University, Tehran, Iran. His research interests include land cover mapping, MODIS LST downscaling, map accuracy assessment, and big remotely sensed data processing.

Hossein Aghighi received the B.Sc. degree in natural resource engineering from the Gorgan University of Agricultural Sciences and Natural Resource, Golestan, Iran, in 2000, the M.Sc. degree in remote sensing and GIS from Tarbiat Modares University, Tehran, Iran, in 2012, and the Ph.D. degree in remote sensing from The University of New South Wales, Sydney, NSW, Australia, in 2015.

He is currently an Assistant Professor with the Remote Sensing and GIS Research Center, Shahid Beheshti University, Tehran. His research interests include remote sensing data processing and applications (optical, LiDAR, and radar), retrieval of vegetation biophysical and biochemical parameters from RS data, Internet of Things, and convergence and synergism between RS, GIS, and IOT for precision farming.

Mohsen Azadbakht received the B.S. degree from Lorestan University, Khorramabad, Iran, and M.S. degrees, from Shahid Beheshti University, Tehran, Iran, in 2004 and 2009, respectively, both in pure mathematics and remote sensing, and the Ph.D. degree in geomatic engineering from the University of Melbourne, Melbourne, VIC, Australia, in 2016.

He is currently an Assistant Professor with Center for Remote Sensing and GIS Research, Shahid Beheshti University, Tehran, Iran. His research interests include remote sensing data processing and applications.

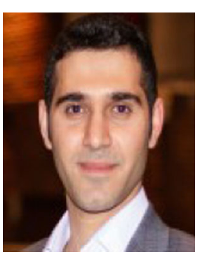

Meisam Amani (Senior Member, IEEE) received the B.Eng. degree in geomatics engineering from University of Tabriz, Tabriz, Iran, in 2012, the M. Eng. degree in remote sensing engineering from K.N. Toosi University of Technology, Tehran, Iran, in 2014, and the Ph.D. degree in electrical engineering from Memorial University of Newfoundland, St. John's, NL, Canada, in 2018.

He is currently a Senior Remote Sensing Engineer and the Key Specialty Leader of Data Analytics with a global consulting and engineering company, called Wood PLC, where he manages and leads various industrial, governmental, and academic remote sensing projects worldwide. Over the past 11 years, he has worked on different applications of remote sensing, including but not limited to land cover/land use classification, soil moisture estimation, drought monitoring, water quality assessment, watershed management, power/transmission line monitoring, fog detection and nowcasting, and ocean wind estimation. To do these, he has utilized various remote sensing datasets (e.g., UAV, optical, LiDAR, SAR, scatterometer, radiometer, and altimeter) along with different machine learning, and big data processing algorithms.

Dr. Amani is an Associate Editor for the IEEE JOURNAL OF SELECTED TOPICS IN APPLIED EARTH OBSERVATIONS AND REMOTE SENSING and the lead Guest Editor for a special issue in the *Remote Sensing* journal. He is also a regular Reviewer in about 15 international remote sensing journals. He was the recipient of the prestigious Professional Engineers and Geoscientists Newfoundland and Labrador Environmental Award, in 2020 due to his contribution to wetland mapping in Canada using advanced machine learning and big data processing algorithms. A list of his research works, including over 50 peer-reviewed journal and conference papers, can be found at https://www.researchgate.net/profile/Meisam_Amani3.

Sahel Mahdavi received the Ph.D. degree in electrical engineering from Memorial University of Newfoundland, St. John's, NL, Canada, in 2018.

Having almost ten years of academic and industrial background in remote sensing, she is familiar with a wide array of topics relevant to RS/GIS and their applications in various environmental aspects. She also co-authored a book entitled *Principles of SAR Remote Sensing.* She has authored more than 40 peer-reviewed journals. She was a member of a provincial project on wetland classification during the Ph.D. when she identified the problem with wetland classification using Remote Sensing and, subsequently, proposed a novel scheme for wetland mapping. She is currently affiliated with the Data Analytics team at Wood PLC. Her research interests include object-based wetland classification using a combination of optical and full-polarimetric SAR data, feature selection, soil moisture retrieval using SAR images, image segmentation, speckle reduction in SAR images, target detection in multispectral optical images, and the relationship between environmental conditions and SAR images.

Dr. Mahdavi is the recipient of the Professional Engineers and Geoscientists Newfoundland and Labrador Environmental Award (2020), the Emera Graduate Scholarship for Distinctive Women in Engineering for three consecutive years (2016–2018), and Newfoundland and Labrador Branch of Canadian Institute of Geomatics (CIG) Scholarship (2015).

Ali Akbar Matkan received the M.Sc. degree in geography from Tarbiat Modares University, Tehran, Iran and the Ph.D. degree in remote sensing from University of Bristol, Bristol, U.K., in 1992 and 2000, respectively.

He is currently a Professor with Center for Remote Sensing and GIS Research, Shahid Beheshti University, Tehran, Iran. His current research interests include climate change, spectroradiometry of vegetation and information extraction from hyperspectral, and thermal data processing.